Realizing gapped surface states in the magnetic topological insulator MnBi$_{2-x}$Sb$_x$Te$_4$

Wonhee Ko [1], Marek Kolmer [1,*], Jiaqiang Yan,[2] Anh D. Pham,[1] Mingming Fu,[1,3] Felix Lüpke,[1,4] Satoshi Okamoto [2]
Zheng Gai [1], P. Ganesh,[1] and An-Ping Li [1,†]

[1]*Center for Nanophase Materials Sciences, Oak Ridge National Laboratory, Oak Ridge, Tennessee 37831, USA*
[2]*Materials Science and Technology Division, Oak Ridge National Laboratory, Oak Ridge, Tennessee 37831, USA*
[3]*Fujian Provincial Key Laboratory of Semiconductors and Applications, Collaborative Innovation Center for Optoelectronic Semiconductors and Efficient Devices, Department of Physics, Xiamen University, Xiamen, Fujian Province 361005, People's Republic of China*
[4]*Department of Materials Science and Engineering, University of Tennessee, Knoxville, Tennessee 37916, USA*

The interplay between magnetism and nontrivial topology in magnetic topological insulators (MTIs) is expected to give rise to exotic topological quantum phenomena like the quantum anomalous Hall effect and the topological axion states. A key to assessing these novel properties is to realize gapped topological surface sates. MnBi$_2$Te$_4$ possesses nontrivial band topology with an intrinsic antiferromagnetic state. However, the highly electron-doped nature of the MnBi$_2$Te$_4$ crystals obstructs the exhibition of the surface band gap. Here, we tailor the material through Sb substitution to reveal the gapped surface states in MnBi$_{2-x}$Sb$_x$Te$_4$. By shifting the Fermi level into the bulk band gap, we access the surface states and show a band gap of 50 meV at the Dirac point from quasiparticle interference measured by scanning tunneling microscopy (STM). Surface-dominant conduction is confirmed through transport spectroscopy measured by multiprobe STM below the Néel temperature. The surface band gap is robust against the out-of-plane magnetic field despite the promotion of field-induced ferromagnetism. The realization of bulk-insulating MTIs with the large exchange gap offers a promising platform for exploring emergent topological phenomena.

I. INTRODUCTION

Magnetic topological insulators (MTIs) possessing naturally gapped surface states provide a central platform for various topological quantum phenomena [1,2]. MnBi$_2$Te$_4$ is an MTI with inverted band structure from large spin-orbit coupling and intrinsic magnetism from Mn magnetic moments [3–5]. The crystal has layered structure with septuple layers (SLs) of Te-Bi-Te-Mn-Te-Bi-Te [inset of Fig. 1(a)]. Below the Néel temperature, magnetic moments of Mn atoms form *A*-type antiferromagnetic (AFM) ordering where they align ferromagnetically in the same layer and antiferromagnetically between adjacent layers [6,7]. The topological nature of the compound was confirmed by observing the topological surface states with angle-resolved photoemission spectroscopy (ARPES) [4,8–13]. However, the abundant bulk carriers and their spatial fluctuations in the highly electron-doped MnBi$_2$Te$_4$ crystals hinder the realization of predicted topological phenomena. For example, previous ARPES studies reported both the existence [4,9,10] and the absence of an exchange gap [11–13] in the topological surface states. Thus, to resolve the fine structures of the band around the Dirac point, it is necessary to control the carrier density and use local spectroscopic techniques like scanning tunneling microscopy/spectroscopy (STM/STS) [14–16].

To compensate the electron carriers in the bulk, thin films of MnBi$_2$Te$_4$ were adapted to reduce bulk carriers and back gating was used to shift the Fermi level inside the gap. Based on this approach, the transport measurements indeed demonstrated crucial characteristics of MTI such as the quantum anomalous Hall (QAH) effect [17] and axion insulator states [18]. However, geometrical effects like interaction between the top and bottom surfaces can alter the topology of the system [19], and impurities and defects introduced during the exfoliation or the epitaxial growth limit the film quality [20]. On the other hand, an approach based on bulk single crystals and *in situ* characterization can overcome these issues to offer a system with higher quality. In particular, substituting Bi with Sb provides a means to introduce hole doping [8,21], and the change in the composition of MnBi$_{2-x}$Sb$_x$Te$_4$ (MBST) enables us to alter the topological phases as well [Fig. 1(a)]. For example, topological phase transitions are expected in increasing Sb composition x, where the topologically nontrivial band of MnBi$_2$Te$_4$ becomes topologically trivial like MnSb$_2$Te$_4$ [8]. In addition, magnetic structure of MBST can change with composition [22]. Topological phase transitions are predicted for different magnetic structures such as topological insulators (TIs) or AFM TIs for AFM structures and ferromagnetic (FM) insulators or Weyl semimetals (WSMs) for FM structures [3,5]. Therefore, shifting the Fermi level into the exchange gap through tailoring the MBST composition offers a key not just to accessing the surface band structures but also to unlocking emergent quantum properties of intrinsic MTIs.

In this paper, we employ Sb substitution to shift the Fermi level of MBST into the bulk band gap and utilize

---
*Current address: Ames Laboratory - U.S. Department of Energy, Ames, Iowa 50011, USA.
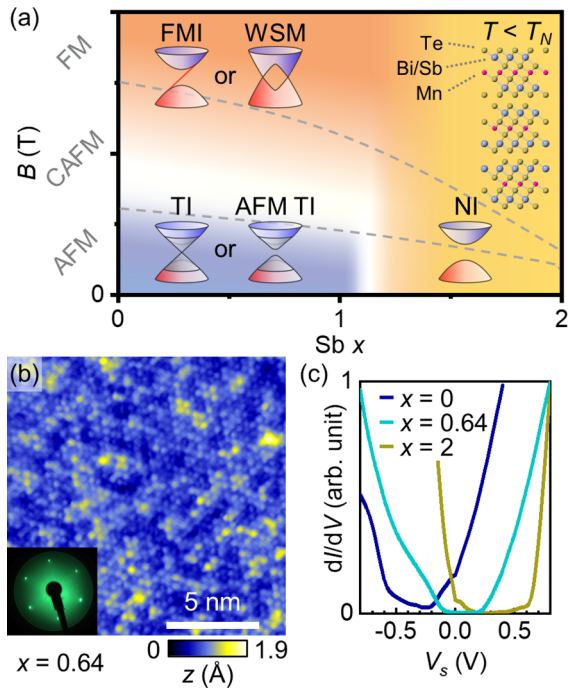†Corresponding author: apli@ornl.gov

FIG. 1. (a) Schematic phase diagram of MBST with respect to Sb composition x and magnetic field B. Inset on the right shows the MBST lattice structure. (b) STM image of MBST with $x = 0.64$ ($V_s = -0.15$ V, $I = 100$ pA). Inset shows the LEED image at 60 eV. (c) dI/dV spectra for MBST crystals with different compositions. Each curve represents the average of about 1000 spectra taken over the area of 30×30 nm^2 (set point $V_s = -1$ V, $I = 500$ pA for $x = 0$; $V_s = 1.5$ V, $I = 100$ pA for $x = 0.64$; $V_s = -0.2$ V, $I = 500$ pA for $x = 2$).

STM-based spectroscopy to demonstrate the gapped surface states. A surface band gap of 50 meV is revealed by quasiparticle interference (QPI) measurement in the bulk-insulating MBST. Density functional theory (DFT) calculations reproduce the gapped surface states and confirm MBST as an AFM TI. The surface nature of the QPI-revealed bands is further corroborated by *in situ* transport spectroscopy with multiprobe STM. Both the bulk and surface band structures are found robust against out-of-plane magnetic field, even though the simultaneous magnetostriction measurement with STM displays a field-induced AFM to FM transition. DFT simulations indicate that the MBST has a ferrimagnetic structure and is a topological axion insulator with $Z_4 = 2$.

II. RESULTS AND DISCUSSION

A. STM/STS on MBST

To study different topological phases, we chose three MBST compositions of $x = 0$, 0.64, and 2. Here, $x = 0$ and 2 represent the exemplary cases of topological and trivial compounds, respectively [Fig. 1(a)], and $x = 0.64$ represents the bulk-insulating case, whose insulating behavior was confirmed by transport measurements (Fig. S1 of the Supplemental Material [23]) [8,21]. Figure 1(b) shows a typical topographic image of the cleaved surface of MBST, which displays triangular lattice of the topmost Te layer. Surface corrugation of ± 1 Å indicates the existence of defects, prob-

ably vacancies, interstitials, and antisites typically observed in Bi-based topological insulators [24–26]. The long-range crystallinity of the surface is confirmed by low-energy electron diffraction (LEED) displaying hexagonal patterns [inset of Fig. 1(b)]. The effect of Sb substitution is examined by taking dI/dV spectra at $T = 4$ K [Fig. 1(c)], which is well below the Néel temperature $T_N \approx 20$ K [6,7,21]. As expected, hole doping from Sb shifts the spectra toward the higher bias with increasing x. The spectrum for $x = 0$ shows V-shaped curves of typical TIs [27–29], while the spectrum for $x = 2$ shows U-shaped curves with a flat zero amplitude region which is typical for trivial normal insulators (NIs) [30]. For the $x = 0$ compound, however, the surface band gap cannot be determined because the whole spectrum is elevated to a nonzero value due to carriers from the highly n-doped bulk. In contrast, for the $x = 0.64$ compound, the spectrum displays a flat bottom with nearly zero dI/dV conductance around the Fermi level, enabling assessment of the surface band gap. The qualitatively different shapes of spectra are not from the difference in set point bias voltages and currents, as examined with different set points for all three compounds in Fig. S2 of the Supplemental Material [23].

B. QPI of MBST with different compositions

QPI is a powerful technique that can provide momentum information of electronic bands based on maps of dI/dV spectra. It also allows for identification of nontrivial topology of the surface states manifested as the prohibition of backscattering due to the spin-momentum locking [31–34]. Several STM studies confirmed strong suppressions of QPI near the Dirac point where the surface bands have the ideal shape of a Dirac cone, while the QPI signals reappear when the energy moves far from the Dirac point and the surface bands start to distort [24,27–29,35–37]. Further application of QPI in extrinsic magnetic topological insulators revealed both the topological surface states and the band gap of surface states [37].

To evaluate the surface band gap, we employed the QPI measurement to reveal surface electronic structures [38] for different MBST compositions (see the movies in the Supplemental Material [23]). Figure 2 displays the line cuts of the QPI maps along the $\bar{\Gamma}$-$\bar{K}$ and $\bar{\Gamma}$-$\bar{M}$ directions in the Brillouin zone that are stacked vertically in energy. The stacking plot displays dispersions in QPI maps that correspond to bulk and surface bands with distinct band gaps E_{bg} and E_{sg}, respectively [37]. The QPI map of the $x = 0$ compound [Fig. 2(a)] shows strong intensity of dispersing bands at $E < -0.53$ eV and $E > -0.25$ eV which presumably correspond to the bulk valence and conduction bands, respectively. Inside the bulk band gap, there is another dispersing band. We attribute this QPI signal to the topological surface states based on the absence of pronounced intensity spots because of prohibited backscattering [24,27,29,37] and the matching dispersion with the expected backscattering q from ARPES results [11] (see Sec. 5 in the Supplemental Material [23]). However, a significant background signal from bulk carriers makes it hard to determine the surface band gap around the Dirac point at $E = -0.31$ eV. In contrast, the $x = 2$ compound [Fig. 2(c)] shows an E_{bg} at 0.18 eV $< E < 0.36$ eV without any dispersing surface bands inside as expected for trivial NIs. Interestingly,
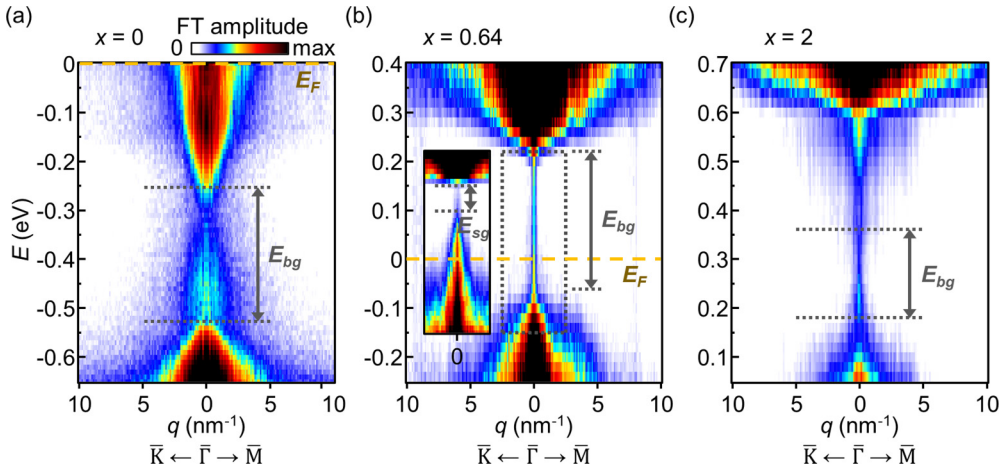
FIG. 2. (a)–(c) Line cuts of QPI along $\bar{\Gamma}$-$\bar{K}$ and $\bar{\Gamma}$-$\bar{M}$ directions stacked in energy for MBST with $x = 0, 0.64$, and 2, respectively (set point $R_T = 0.81, 1.67$, and 0.4 GΩ, respectively). The energy of states E relative to the Fermi energy E_F is calculated as $E - E_F = eV_s$. Inset in (b) shows the QPI taken with the STM tip closer to the surface (set point $R_T = 1$ GΩ).

the $x = 0.64$ compound [Fig. 2(b)] exhibits the bulk band dispersion at $E < -0.08$ eV and $E > 0.2$ eV with more pronounced bulk band gap due to the large reduction of the bulk carrier density. Still, when the STM tip is brought closer to the surface, dI/dV spectra show a finite signal inside E_{bg} [Fig. S2(a) in [23]], and the QPI map reveals additional dispersing bands too [inset of Fig. 2(b)]. We attribute these bands to the topological surface state which is gapped, because two almost linearly dispersing bands form a Dirac-cone-like structure with strongly reduced intensity at the crossing point. These emerging bands do not originate from external effects, such as the tip-induced band bending of the bulk bands [30,39,40], as verified by various tip height set points (Fig. S3 in [23]). At the Dirac point, the surface band shows a clear gap of $E_{sg} = 50$ meV as a featureless QPI region [inset of Fig. 2(b)] [37]. DFT calculations for the $x = 0.64$ compound show the existence of nontrivial topological phase with A-type AFM coupling (Fig. S6 in [23]) and reproduce the surface band gap with size of about 40 meV on the (111)-projected surface (Fig. S7 in [23]). The gap is due to uncompensated magnetic moments on the surface that break both time-reversal and translational symmetries, while the projected surface states on the (110) surface still retain the gapless Dirac dispersion (Fig. S8 in [23]). The good agreement between STM observations and DFT calculations allows us to conclude that the bulk band of the $x = 0.64$ compound is inverted and the topological surface states on the (111) surface are gapped [3–5,41].

C. Differentiation of bulk and surface transport in MBST with four-probe STM

To further confirm the surface nature of the electronic states at the Fermi level in bulk-insulating MBST, we measured surface transport with a multiprobe STM [42]. We employed a variable probe-spacing transport spectroscopy based on the multiprobe STM, which was developed to efficiently differentiate the bulk and surface conductance [43–45]. Briefly, four-probe resistance R is measured while

varying probe distances [inset of Fig. 3(a)], and the resulting plot of R versus X_g is fitted to a linear relationship to obtain a fitting parameter $g \equiv s_{14}.\rho_{2D}/\rho_{3D}$ which measures the ratio of bulk to surface conductivity (see Sec. 1 in the Supplemental Material [23]) [43]. Figure 3(a) shows the results of variable probe-spacing spectroscopy for the $x = 0$ compound at $T = 82$ K. The fitted $g = 35.5$, indicating that 97% of the conductivity comes from the bulk channel. The bulk dominant conductance and the obtained bulk resistivity $\rho_{3D} = 3.04$ mΩ cm are consistent with bulk behaviors measured by a physical property measurement system (PPMS) [7,21]. In contrast, the measurement on the $x = 0.64$
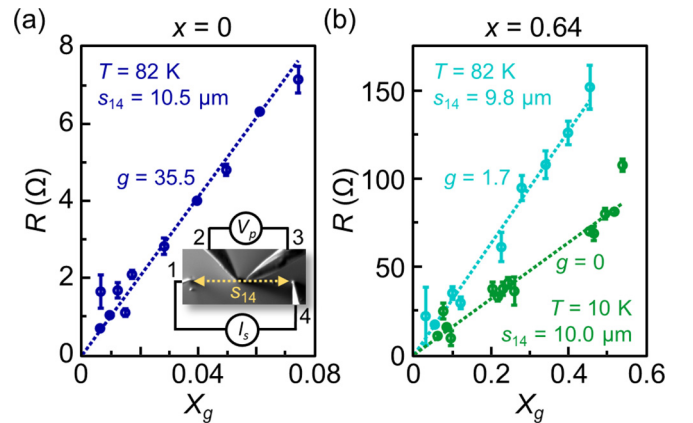

FIG. 3. (a) The $x = 0$ compound shows bulk-dominant conduction. Linear fitting of R-X_g graph taken at $T = 82$ K (dotted line) gives rise to $g = 35.5$ with $\rho_{3D} = 3.04$ mΩ cm and $\rho_{2D} = 102$ Ω. Inset is an SEM image with the schematic of variable probe-spacing four-probe STM measurement (image size 24.5×12 μm^2). (b) The $x = 0.64$ compound shows surface-dominant conduction with a bulk-insulating behavior. Linear fittings of the graphs (dotted lines) give rise to $g = 1.7$, $\rho_{3D} = 182$ mΩ cm and $\rho_{2D} = 318$ Ω at $T = 82$ K, and $g = 0$, $\rho_{3D} > 1590$ mΩ cm and $\rho_{2D} = 159$ Ω at $T = 10$ K.
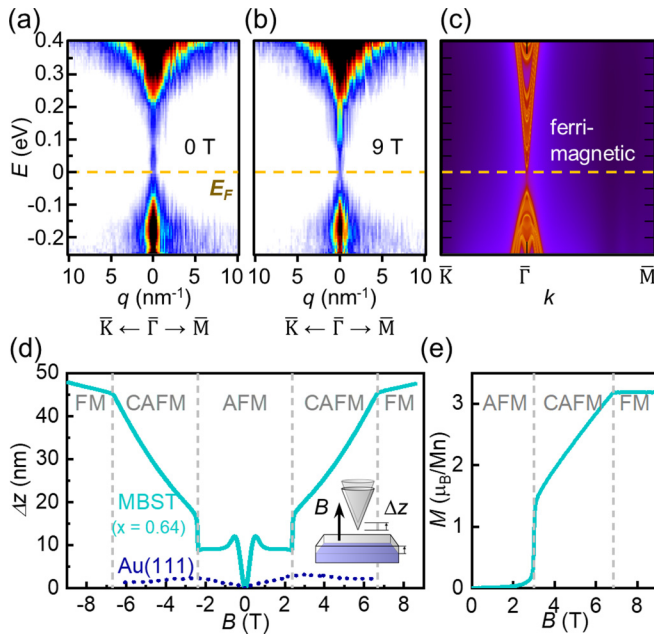
FIG. 4. (a), (b) QPI measured at 0 and 9 T, respectively (set point $R_T = 0.3\,\mathrm{G\Omega}$). (c) DFT calculations of the band structure as projected to (111) surface of $x = 0.64$ compound in the ferrimagnetic state. (d) Magnetostriction measured with STM. Inset shows the scheme of the measurement. (e) The c-axis magnetization measured *ex situ* with PPMS for $x = 0.63$ compound. (Adapted with permission from Ref. [21]. Copyright 2019 by the American Physical Society.)

compound at $T = 82\,\mathrm{K}$ gives rise to $g = 1.7$, which indicates that the portion of the surface conductivity has increased to 37% [Fig. 3(b)]. Furthermore, we find $g = 0$ at 10 K, namely 100% of the conduction comes from the surface channel. The decrease in temperature is found to increase ρ_{3D} and decrease ρ_{2D} (see Fig. 3 caption for their values), which is consistent with the expected behaviors of TIs [45]. The results provide direct confirmation on the bulk-insulating behavior of $x = 0.64$ compound and the existence of the topological surface states, corroborating well with the QPI results.

D. Magnetic field effect on the electronic structure of MBST

To gain insight into the effect of magnetic structure on the topological phases of MBST, we performed QPI measurements in magnetic field. Applying 9-T out-of-plane magnetic field is expected to change the interlayer AFM order to FM and suppress the anisotropic fluctuations of the local magnetic moments [21]. QPI maps taken at both 0 and 9 T at the same surface location of the $x = 0.64$ compound are comparatively shown in Figs. 4(a) and 4(b), respectively. The dispersion relations for both the bulk conduction band at $E > 0.2\,\mathrm{eV}$ and valence band at $E < -0.05\,\mathrm{eV}$ are almost identical for both cases, which shows the robustness of the band structure against the magnetic field. The size of the bulk band gap remains unchanged in magnetic field, indicating that the field-induced FM state is an insulator rather than a WSM [3,5]. We note that both Figs. 4(a) and 4(b) show QPI signal minimal at

0–0.05 eV, consistent with the measured 50-meV surface band gap, although the weak QPI signal of the surface states makes it hard to resolve the fine structures around the Dirac point at high magnetic field. In addition, the surface states do not show any change in dI/dV spectra as the magnetic field increases from 0 to 8.5 T for the $x = 0$ compound (Fig. S5 in [23]) [15]. Therefore, both the bulk and surface states are robust against the out-of-plane magnetic field.

The field-induced AFM to FM transition in MBST is further examined in a magnetostriction effect detected by STM. Magnetostriction comes from magnetoelastic coupling that causes a change in dimensions in response to varying net magnetization in magnetic materials [46]. To detect the magnetostriction, the STM tip was held in the constant current mode, and the change in tip height Δz was recorded while ramping the out-of-plane magnetic field B [inset of Fig. 4(d)]. With the increase of B, Δz shows large jumps at ± 2.4 T and clear kinks at ± 6.7 T. These transition points match well the behaviors measured with PPMS as shown in Fig. 4(e), where magnetic transitions occur sequentially from AFM to CAFM and then to FM states [21]. The change of Δz is mainly due to the magnetoelastic coupling in MBST since much smaller variations in Δz are observed by repeating the measurement on a nonmagnetic Au(111). An additional drop in Δz of MBST at 0 T may come from mechanical distortion of the STM stage in response to the magnetic field, since the similar drop, though with smaller magnitude, also occurs to the Au(111).

To understand the topological phases of the MBST in the field-induced FM state, we employed DFT calculations and considered the two different magnetic configurations: FM and ferrimagnetic. Because the measured magnetic moment of Mn in Fig. 4(e) is less than the theoretical prediction of $4-5\,\mu_B/\mathrm{Mn}$ for $\mathrm{Mn^{2+}}$ [4,5,21], we considered the ferrimagnetic case where 1/3 of Mn ions couple antiferromagnetically with the majority of Mn (Fig. S15 in [23]). For the FM case, the $x = 0.64$ compound with bulk experimental lattice parameters is a normal semimetal with zero Chern number (Fig. S9 in [23]). However, in the ferrimagnetic configuration, the $x = 0.64$ compound contains a clear gap [Fig. 4(c)]. The finite bulk band gap is similar to the AFM configuration but the Chern number is a zero (Fig. S10 in [23]) and the corresponding (111) surface shows a surface band gap.

We further investigated the topologies of the FM and ferrimagnetic configurations. Both FM and ferrimagnetic $\mathrm{MnBi_2Te_4}$ have band inversion between Bi-p and Te-p states at the Γ point, but their Chern numbers equal zero (Figs. S11 and S12 in [23]). Since the band inversion indicates nontrivial topology, we further calculated the Z_4 value and found $Z_4 = 2$ (Tables S1 and S2 in [23]) [47], which indicates that both FM and ferrimagnetic $\mathrm{MnBi_2Te_4}$ are a topological axion insulator with gapped surfaces on both (111) and (110) surfaces (Figs. S13 and S14 in [23]). The results suggest that $x = 0.64$ compound in magnetic field is also most likely an axion insulator since our alloy model from virtual crystal approximation preserves inversion symmetry in $\mathrm{MnBi_2Te_4}$. As a result, a transition between two nontrivial topological phases of AFM and ferrimagnetic states would not require a closing of bulk or surface band gap [48].

III. CONCLUSION

In conclusion, by tuning the Fermi level of MBST into the bulk band gap we reveal a surface band gap of 50 meV in the QPI measurement, which is corroborated by multiprobe STM transport spectroscopy and DFT calculations. The good agreement between STM and DFT analyses suggests that the surface magnetic structure remains as *A*-type AFM [12,49]. Both the surface and bulk band gaps remain unchanged in both AFM and FM states, excluding a possible transition to a WSM and suggesting a topological axion insulator in the field-induced FM state. The results provide understanding on the recent demonstration of QAH and axion states which require gapped topological surface states [17,18], and the absence of chiral anomaly that should exist in WSMs [10]. The large topological surface band gap of MBST would facilitate the applications for quantum information sciences, such as topological quantum computation with the Majorana bound states at the interface between QAH states and superconductors [50,51].

[1] Y. Tokura, K. Yasuda, and A. Tsukazaki, Magnetic topological insulators, Nat. Rev. Phys. **1**, 126 (2019).

[2] C. X. Liu, S. C. Zhang, and X. L. Qi, The quantum anomalous hall effect: Theory and experiment, Annu. Rev. Condens. Matter Phys. **7**, 301 (2016).

[3] D. Zhang, M. Shi, T. Zhu, D. Xing, H. Zhang, and J. Wang, Topological Axion States in the Magnetic Insulator MnBi$_2$Te$_4$ with the Quantized Magnetoelectric Effect, Phys. Rev. Lett. **122**, 206401 (2019).

[4] M. M. Otrokov, I. I. Klimovskikh, H. Bentmann, D. Estyunin, A. Zeugner, Z. S. Aliev, S. Gaß, A. U. B. Wolter, A. V. Koroleva, A. M. Shikin, M. Blanco-Rey, M. Hoffmann, I. P. Rusinov, A. Y. Vyazovskaya, S. V. Eremeev, Y. M. Koroteev, V. M. Kuznetsov, F. Freyse, J. Sánchez-Barriga, I. R. Amiraslanov *et al.*, Prediction and observation of an antiferromagnetic topological insulator, Nature (London) **576**, 416 (2019).

[5] J. Li, Y. Li, S. Du, Z. Wang, B. L. Gu, S. C. Zhang, K. He, W. Duan, and Y. Xu, Intrinsic magnetic topological insulators in van der Waals layered MnBi$_2$Te$_4$-family materials, Sci. Adv. **5**, eaaw5685 (2019).

[6] P. Rani, A. Saxena, R. Sultana, V. Nagpal, S. S. Islam, S. Patnaik, and V. P. S. Awana, Crystal Growth and Basic Transport and Magnetic Properties of MnBi$_2$Te$_4$, J. Supercond. Nov. Magn. **32**, 3705 (2019).

[7] J. Q. Yan, Q. Zhang, T. Heitmann, Z. Huang, K. Y. Chen, J. G. Cheng, W. Wu, D. Vaknin, B. C. Sales, and R. J. McQueeney, Crystal growth and magnetic structure of MnBi$_2$Te$_4$, Phys. Rev. Mater. **3**, 064202 (2019).

[8] B. Chen, F. Fei, D. Zhang, B. Zhang, W. Liu, S. Zhang, P. Wang, B. Wei, Y. Zhang, Z. Zuo, J. Guo, Q. Liu, Z. Wang, X. Wu, J. Zong, X. Xie, W. Chen, Z. Sun, S. Wang, Y. Zhang *et al.*, Intrinsic magnetic topological insulator phases in the Sb doped MnBi$_2$Te$_4$ bulks and thin flakes, Nat. Commun. **10**, 4469 (2019).

[9] R. C. Vidal, H. Bentmann, T. R. F. Peixoto, A. Zeugner, S. Moser, C. H. Min, S. Schatz, K. Kißner, M. Ünzelmann, C. I. Fornari, H. B. Vasili, M. Valvidares, K. Sakamoto, D. Mondal, J. Fujii, I. Vobornik, S. Jung, C. Cacho, T. K. Kim, R. J. Koch *et al.*, Surface states and Rashba-type spin polarization in antiferromagnetic MnBi$_2$Te$_4$ (0001), Phys. Rev. B **100**, 121104 (2019).

[10] S. H. Lee, Y. Zhu, Y. Wang, L. Miao, T. Pillsbury, H. Yi, S. Kempinger, J. Hu, C. A. Heikes, P. Quarterman, W. Ratcliff, J. A. Borchers, H. Zhang, X. Ke, D. Graf, N. Alem, C.-Z. Chang, N. Samarth, and Z. Mao, Spin scattering and noncollinear spin structure-induced intrinsic anomalous Hall effect in antiferromagnetic topological insulator MnBi$_2$Te$_4$, Phys. Rev. Res. **1**, 012011 (2019).

[11] Y. J. Chen, L. X. Xu, J. H. Li, Y. W. Li, H. Y. Wang, C. F. Zhang, H. Li, Y. Wu, A. J. Liang, C. Chen, S. W. Jung, C. Cacho, Y. H. Mao, S. Liu, M. X. Wang, Y. F. Guo, Y. Xu, Z. K. Liu, L. X. Yang, and Y. L. Chen, Topological Electronic Structure and Its Temperature Evolution in Antiferromagnetic Topological Insulator MnBi$_2$Te$_4$, Phys. Rev. X **9**, 041040 (2019).

[12] Y.-J. Hao, P. Liu, Y. Feng, X.-M. Ma, E. F. Schwier, M. Arita, S. Kumar, C. Hu, R. e. Lu, M. Zeng, Y. Wang, Z. Hao, H.-Y. Sun, K. Zhang, J. Mei, N. Ni, L. Wu, K. Shimada, C. Chen, Q. Liu, and C. Liu, Gapless Surface Dirac Cone in Antiferromagnetic Topological Insulator MnBi$_2$Te$_4$, Phys. Rev. X **9**, 041038 (2019).

[13] H. Li, S.-Y. Gao, S.-F. Duan, Y.-F. Xu, K.-J. Zhu, S.-J. Tian, J.-C. Gao, W.-H. Fan, Z.-C. Rao, J.-R. Huang, J.-J. Li, D.-Y. Yan, Z.-T. Liu, W.-L. Liu, Y.-B. Huang, Y.-L. Li, Y. Liu, G.-B. Zhang, P. Zhang, T. Kondo *et al.*, Dirac Surface States in Intrinsic Magnetic Topological Insulators EuSn$_2$As$_2$ and MnBi$_{2n}$Te$_{3n+1}$, Phys. Rev. X **9**, 041039 (2019).

[14] E. Kotta, L. Miao, Y. Xu, S. A. Breitweiser, C. Jozwiak, A. Bostwick, E. Rotenberg, W. Zhang, W. Wu, T. Suzuki, J. Checkelsky, and L. A. Wray, Spectromicroscopic measurement of surface and bulk band structure interplay in a disordered topological insulator, Nat. Phys. **16**, 285 (2020).

[15] Y. Yuan, X. Wang, H. Li, J. Li, Y. Ji, Z. Hao, Y. Wu, K. He, Y. Wang, Y. Xu, W. Duan, W. Li, and Q. K. Xue, Electronic states

and magnetic response of MnBi$_2$Te$_4$ by scanning tunneling microscopy and spectroscopy, Nano Lett. **20**, 3271 (2020).

[16] Z. Liang, M. Shi, Q. Zhang, S. Nie, J.-J. Ying, J.-F. He, T. Wu, Z. Wang, Z. Wang, and X.-H. Chen, Mapping the Dirac fermions in intrinsic antiferromagnetic topological insulators (MnBi$_2$Te$_4$)(Bi$_2$Te$_3$)$_n$(n = 0, 1), arXiv:2001.00866.

[17] Y. Deng, Y. Yu, M. Z. Shi, Z. Guo, Z. Xu, J. Wang, X. H. Chen, and Y. Zhang, Quantum anomalous Hall effect in intrinsic magnetic topological insulator MnBi$_2$Te$_4$, Science **367**, 895 (2020).

[18] C. Liu, Y. Wang, H. Li, Y. Wu, Y. Li, J. Li, K. He, Y. Xu, J. Zhang, and Y. Wang, Robust axion insulator and Chern insulator phases in a two-dimensional antiferromagnetic topological insulator, Nat. Mater. **19**, 522 (2020).

[19] Y. Zhang, K. He, C. Z. Chang, C. L. Song, L. L. Wang, X. Chen, J. F. Jia, Z. Fang, X. Dai, W. Y. Shan, S. Q. Shen, Q. Niu, X. L. Qi, S. C. Zhang, X. C. Ma, and Q. K. Xue, Crossover of the three-dimensional topological insulator Bi$_2$Se$_3$ to the two-dimensional limit, Nat. Phys. **6**, 584 (2010).

[20] Y. Gong, J. Guo, J. Li, K. Zhu, M. Liao, X. Liu, Q. Zhang, L. Gu, L. Tang, X. Feng, D. Zhang, W. Li, C. Song, L. Wang, P. Yu, X. Chen, Y. Wang, H. Yao, W. Duan, Y. Xu *et al.*, Experimental realization of an intrinsic magnetic topological insulator, Chin. Phys. Lett. **36**, 076801 (2019).

[21] J. Q. Yan, S. Okamoto, M. A. McGuire, A. F. May, R. J. McQueeney, and B. C. Sales, Evolution of structural, magnetic, and transport properties in MnBi$_{2-x}$Sb$_x$Te$_4$, Phys. Rev. B **100**, 104409, (2019).

[22] T. Murakami, Y. Nambu, T. Koretsune, G. Xiangyu, T. Yamamoto, C. M. Brown, and H. Kageyama, Realization of interlayer ferromagnetic interaction in MnSb$_2$Te$_4$ toward the magnetic Weyl semimetal state, Phys. Rev. B **100**, 195103, (2019).

[23] See Supplemental Material at http://link.aps.org/supplemental/10.1103/PhysRevB.102.115402 for methods, additional STM data, and DFT calculations, and for additional references [52–57].

[24] H. Beidenkopf, P. Roushan, J. Seo, L. Gorman, I. Drozdov, Y. S. Hor, R. J. Cava, and A. Yazdani, Spatial fluctuations of helical Dirac fermions on the surface of topological insulators, Nat. Phys. **7**, 939 (2011).

[25] J. Dai, D. West, X. Wang, Y. Wang, D. Kwok, S. W. Cheong, S. B. Zhang, and W. Wu, Toward the Intrinsic Limit of the Topological Insulator Bi$_2$Se$_3$, Phys. Rev. Lett. **117**, 106401 (2016).

[26] K. L. Scipioni, Z. Wang, Y. Maximenko, F. Katmis, C. Steiner, and V. Madhavan, Role of defects in the carrier-tunable topological-insulator (Bi$_{1-x}$Sb$_x$)$_2$Te$_3$ thin films, Phys. Rev B **97**, 125150 (2018).

[27] Z. Alpichshev, J. G. Analytis, J. H. Chu, I. R. Fisher, Y. L. Chen, Z. X. Shen, A. Fang, and A. Kapitulnik, STM Imaging of Electronic Waves on the Surface of Bi$_2$Te$_3$: Topologically Protected Surface States and Hexagonal Warping Effects, Phys. Rev. Lett. **104**, 016401 (2010).

[28] S. Kim, M. Ye, K. Kuroda, Y. Yamada, E. E. Krasovskii, E. V. Chulkov, K. Miyamoto, M. Nakatake, T. Okuda, Y. Ueda, K. Shimada, H. Namatame, M. Taniguchi, and A. Kimura, Surface Scattering Via Bulk Continuum States in the 3D Topological Insulator Bi$_2$Se$_3$, Phys. Rev. Lett. **107**, 056803 (2011).

[29] W. Ko, I. Jeon, H. W. Kim, H. Kwon, S. J. Kahng, J. Park, J. S. Kim, S. W. Hwang, and H. Suh, Atomic and electronic structure of an alloyed topological insulator, Bi$_{1.5}$Sb$_{0.5}$Te$_{1.7}$Se$_{1.3}$, Sci. Rep. **3**, 2656 (2013).

[30] R. M. Feenstra, A prospective: Quantitative scanning tunneling spectroscopy of semiconductor surfaces, Surf. Sci. **603**, 2841 (2009).

[31] L. Fu, Hexagonal Warping Effects in the Surface States of the Topological Insulator Bi$_2$Te$_3$, Phys. Rev. Lett. **103**, 266801 (2009).

[32] W. C. Lee, C. Wu, D. P. Arovas, and S. C. Zhang, Quasiparticle interference on the surface of the topological insulator Bi$_2$Te$_3$, Phys. Rev. B **80**, 245439 (2009).

[33] H. M. Guo and M. Franz, Theory of quasiparticle interference on the surface of a strong topological insulator, Phys. Rev. B **81**, 041102(R) (2010).

[34] Q. Liu, X. L. Qi, and S. C. Zhang, Stationary phase approximation approach to the quasiparticle interference on the surface of a strong topological insulator, Phys. Rev. B **85**, 125314 (2012).

[35] P. Roushan, J. Seo, C. V. Parker, Y. S. Hor, D. Hsieh, D. Qian, A. Richardella, M. Z. Hasan, R. J. Cava, and A. Yazdani, Topological surface states protected from backscattering by chiral spin texture, Nature (London) **460**, 1106 (2009).

[36] J. Seo, P. Roushan, H. Beidenkopf, Y. S. Hor, R. J. Cava, and A. Yazdani, Transmission of topological surface states through surface barriers, Nature (London) **466**, 343 (2010).

[37] I. Lee, C. K. Kim, J. Lee, S. J. L. Billinge, R. Zhong, J. A. Schneeloch, T. Liu, T. Valla, J. M. Tranquada, G. Gu, and J. C. S. Davis, Imaging Dirac-mass disorder from magnetic dopant atoms in the ferromagnetic topological insulator Cr$_x$(Bi$_{0.1}$Sb$_{0.9}$)$_{2-x}$Te$_3$, Proc. Natl. Acad. Sci. USA **112**, 1316 (2015).

[38] J. E. Hoffman, K. McElroy, D. H. Lee, K. M. Lang, H. Eisaki, S. Uchida, and J. C. Davis, Imaging quasiparticle interference in Bi$_2$Sr$_2$CaCu$_2$O$_{8+\delta}$, Science **297**, 1148 (2002).

[39] R. M. Feenstra, Y. Dong, M. P. Semtsiv, and W. T. Masselink, Influence of tip-induced band bending on tunnelling spectra of semiconductor surfaces, Nanotechnology **18**, 044015, (2007).

[40] G. D. Nguyen, L. Liang, Q. Zou, M. Fu, A. D. Oyedele, B. G. Sumpter, Z. Liu, Z. Gai, K. Xiao, and A. P. Li, 3D Imaging and Manipulation of Subsurface Selenium Vacancies in PdSe$_2$, Phys. Rev. Lett. **121**, 086101, (2018).

[41] R. S. K. Mong, A. M. Essin, and J. E. Moore, Antiferromagnetic topological insulators, Phys. Rev. B **81**, 245209 (2010).

[42] T.-H. Kim, Z. Wang, J. F. Wendelken, H. H. Weitering, W. Li, and A.-P. Li, A cryogenic Quadraprobe scanning tunneling microscope system with fabrication capability for nanotransport research, Rev. Sci. Instrum. **78**, 123701 (2007).

[43] C. Durand, X. G. Zhang, S. M. Hus, C. Ma, M. A. McGuire, Y. Xu, H. Cao, I. Miotkowski, Y. P. Chen, and A. P. Li, Differentiation of surface and bulk conductivities in topological insulators via four-probe spectroscopy, Nano Lett. **16**, 2213 (2016).

[44] S. M. Hus, X. G. Zhang, G. D. Nguyen, W. Ko, A. P. Baddorf, Y. P. Chen, and A. P. Li, Detection of the Spin-Chemical Potential in Topological Insulators Using Spin-Polarized Four-Probe STM, Phys. Rev. Lett. **119**, 137202 (2017).

[45] W. Ko, G. D. Nguyen, H. Kim, J. S. Kim, X. G. Zhang, and A. P. Li, Accessing the Intrinsic Spin Transport in

a Topological Insulator by Controlling the Crossover of Bulk-to-Surface Conductance, Phys. Rev. Lett. **121**, 176801 (2018).

[46] E. W. Lee, Magnetostriction and magnetomechanical effects, Rep. Prog. Phys. **18**, 184 (1955).

[47] C. Hu, L. Ding, K. N. Gordon, B. Ghosh, H. J. Tien, H. Li, A. G. Linn, S. W. Lien, C. Y. Huang, S. Mackey, J. Liu, P. V. S. Reddy, B. Singh, A. Agarwal, A. Bansil, M. Song, D. Li, S. Y. Xu, H. Lin, H. Cao, T. R. Chang, D. Dessau, and N. Ni, Realization of an intrinsic ferromagnetic topological state in $MnBi_8Te_{13}$, Sci. Adv. **6**, eaba4275 (2020).

[48] R. X. Zhang, F. Wu, and S. Das Sarma, Möbius Insulator and Higher-Order Topology in $MnBi_{2n}Te_{3n+1}$, Phys. Rev. Lett. **124**, 136407 (2020).

[49] D. Nevola, H. X. Li, J.-Q. Yan, R. G. Moore, H.-N. Lee, H. Miao, and P. D. Johnson, Coexistence of surface ferromagnetism and gapless topological state in $MnBi_2Te_4$, arXiv:2004.06895.

[50] Q. L. He, L. Pan, A. L. Stern, E. C. Burks, X. Che, G. Yin, J. Wang, B. Lian, Q. Zhou, E. S. Choi, K. Murata, X. Kou, Z. Chen, T. Nie, Q. Shao, Y. Fan, S. C. Zhang, K. Liu, J. Xia, and K. L. Wang, Chiral Majorana fermion modes in a quantum anomalous Hall insulator–superconductor structure, Science **357**, 294 (2017).

[51] M. Kayyalha, D. Xiao, R. Zhang, J. Shin, J. Jiang, F. Wang, Y. F. Zhao, R. Xiao, L. Zhang, K. M. Fijalkowski, P. Mandal, M. Winnerlein, C. Gould, Q. Li, L. W. Molenkamp, M. H. W. Chan, N. Samarth, and C. Z. Chang, Absence of evidence for chiral Majorana modes in quantum anomalous Hall-superconductor devices, Science **367**, 64 (2020).

[52] J. P. Perdew, K. Burke, and M. Ernzerhof, Generalized Gradient Approximation Made Simple, Phys. Rev. Lett. **77**, 3865 (1996).

[53] S. L. Dudarev, G. A. Botton, S. Y. Savrasov, C. J. Humphreys, and A. P. Sutton, Electron-energy-loss spectra and the structural stability of nickel oxide: An LSDA+U study, Phys. Rev. B **57**, 1505 (1998).

[54] J. Li, C. Wang, Z. Zhang, B.-L. Gu, W. Duan, and Y. Xu, Magnetically controllable topological quantum phase transitions in the antiferromagnetic topological insulator $MnBi_2Te_4$, Phys. Rev. B **100**, 121103 (2019).

[55] Q. Wu, S. Zhang, H.-F. Song, M. Troyer, and A. A. Soluyanov, WannierTools: An open-source software package for novel topological materials, Comput. Phys. Commun. **224**, 405 (2018).

[56] A. A. Mostofi, J. R. Yates, Y.-S. Lee, I. Souza, D. Vanderbilt, and N. Marzari, wannier90: A tool for obtaining maximally-localised Wannier functions, Comput. Phys. Commun. **178**, 685 (2008).

[57] J. Gao, Q. Wu, C. Persson, and Z. Wang, Irvsp: to obtain irreducible representations of electronic states in the VASP, arXiv:2002.04032.